archives
of thermodynamics
Vol. **36**(2015), No. 1, 19–38
DOI: 10.1515/aoter-2015-0002

Numerical modeling and preliminary validation of drag-based vertical axis wind turbine

TOMASZ KRYSIŃSKI[1]
ZBIGNIEW BULIŃSKI
ANDRZEJ J. NOWAK

Silesian University of Technology, Institute of Thermal Technology,
Konarskiego 22, 44-100 Gliwice, Poland

Abstract The main purpose of this article is to verify and validate the mathematical description of the airflow around a wind turbine with vertical axis of rotation, which could be considered as representative for this type of devices. Mathematical modeling of the airflow around wind turbines in particular those with the vertical axis is a problematic matter due to the complex nature of this highly swirled flow. Moreover, it is turbulent flow accompanied by a rotation of the rotor and the dynamic boundary layer separation. In such conditions, the key aspects of the mathematical model are accurate turbulence description, definition of circular motion as well as accompanying effects like centrifugal force or the Coriolis force and parameters of spatial and temporal discretization. The paper presents the impact of the different simulation parameters on the obtained results of the wind turbine simulation. Analysed models have been validated against experimental data published in the literature.

Keywords: Numerical modeling; Numerical axis wind turbine; Computational fluid dynamics

Nomenclature

Cp – coefficient of power
Ct – coefficient of torque

[1]Corresponding Author. E-mail: tomasz.krysinski@polsl.pl

D	–	diameter, m
H	–	height, m
p	–	pressure, Pa
Re	–	Reynolds number
t	–	time, s
T	–	integration time, s
TSR	–	tip speed ratio
$\mathbf{u}$	–	velocity, m/s
w	–	wind velocity, m/s
$\mathbf{x}$	–	position vector
$(\bar{\cdot})$	–	time average quantity
$(\cdot)'$	–	fluctuation quantity

Greek symbols

λ	–	tip speed ratio
ρ	–	density, kg/m^3
μ	–	dynamic viscosity, Pas
ν	–	kinematic viscosity, kg/(s*m)
τ	–	shear stress, N/m^2
φ	–	instantaneous flow variable
ω	–	radial velocity, rad/s

1 Introduction

Depending on the orientation of the axis of wind turbine, they can be divided into two basic designs, namely, horizontal axis turbines (horizontal axis wind turbine – HAWT) and the vertical axis turbines (vertical axis wind turbine – VAWT). There are also spacial constructions of turbines with vertical flow of working fluid, a combination of wind turbine and solar collector, but they are less frequent. Although, the origins of the main two designs are dated back to the beginning of twentieth century, more popular are horizontal axis turbines. Many authors explain this state by a significantly higher efficiency of these devices compared to vertical axis turbines [1–3]. However, it is worth noting that the constructions with vertical axis have been forgotten for several decades, while constructions with horizontal axis at this time were widely studied and improved. Some researchers also predict that in the next years the vertical axis turbines will dominate the electricity production sector, due to their significant advantages [4]. The most important among them are: lower noise emission, higher cut off wind speed, lower minimal operational wind speed, low susceptibility on the wind turbulence level, omni-directionality, more compact construction. These are the main reasons for recently growing popularity of VAWT type constructions. To support these predictions, Pope presented

a preliminary analysis of the effectiveness of various options of HAWT and VAWT, in the context of the first and second law of thermodynamics [5].

There is an extensive literature review involving various aspects of wind turbines operation, starting from their aerodynamics, through the structural and mechanical problems, generation of electricity, connection to the power grid and environmental issues [1,2]. However, most of these works are strongly focused on horizontal axis turbines, just only mentioning vertical axis designs. In the last few years, the vertical constructions are experiencing a revival of interest of scientists and engineers. Their operation is subject of intense research, with usage of both experimental and computational methods.

A single stage Savonius rotor was selected for this study as a construction variant of the vertical axis wind turbine, the main selection criterion was the availability of experimental data that could be used for validation. Such a rotor type is a design proposed by the Finnish engineer S.J. Savonius around 1920 [10]. A characteristic feature of this construction is the S-shaped rotor, consisting of two semicylindrical blades.

This paper presents a credibility analysis of the mathematical description, as well as the results of computer simulation of air flow around the wind turbine. Basic methods for modeling are verified, namely a study of different methods to simulate the movement of the rotor (MRF – multiple reference frame method and sliding mesh method), analysis of numerical grid structure influence, time step size for transient simulations and the impact of the choice of turbulence model is included in the presented verification. Especially, influence of listed above parameters on the determination of forces acting on the rotor is investigated.

2 Numerical model of vertical axis wind turbine

2.1 Turbine rotor geometry

The geometry of the rotor is defined as the characteristic shape for the Savonius wind turbines. Hemispherical rotor blades fastened from the top and bottom by the two disks, is arranged in the shape of the 'S' letter. Schematically, the shape and the main dimensions are shown in Fig. 1.
Rotor diameter and the height denoted by D and H were equal to 208 mm. The overlap ratio of the rotor vanes a was set at 15% of the rotor diameter. The thickness of the material forming the rotor blade is 2 mm, while the thickness of the each disc at the top and bottom of the rotor is 10 mm. The

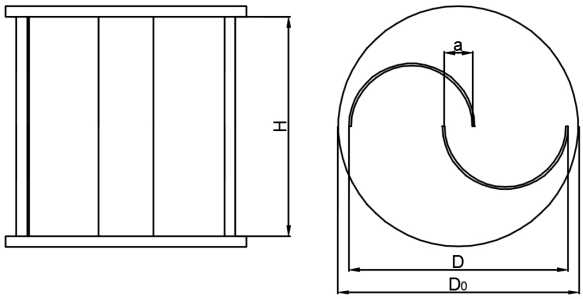

Figure 1: Turbine rotor geometry.

diameter of the blades connecting disk, D_0, was 1.1 D. Rotor geometry used in the described model was experimentally examined by Kamoji *et al.* [6].

The geometric model of the turbine rotor was generated using solid modeling tools in Catia V5R20 environment [11], and then imported to ANSYS ICEM computational fluid dynamics (CFD) meshing software, in which numerical grid was created [12].

2.2 Computational domain and numerical grid

Modeling of wind turbine operation is a fairly complex problem. First of all the computational domain should be defined in such a way that external flow boundary conditions do not affect the final solution. A hexahedron domain was finally assumed in calculations, its shape and dimensions are shown in Fig. 2.

Within the computational domain two separated subvolumes were distinguished. Namely, the bulk volume which is assumed to be stationary and near-rotor volume in which the rotor is immersed. In this region, turbine rotation needs to be modeled with appropriate technique. In order to ensure high quality of computational grid, a hybrid technique was applied. The bulk volume due to its regular and simple shape was filled with hexahedron structural grid. Structural grids accelerate computing, facilitate convergence, as well as reduce numerical solution error. On the other hand, due to the complex shape of the rotor, cylindrical near-rotor volume was meshed with unstructured grid built of tetrahedral elements. In all studied cases maximal size of grid elements (both tetrahedral and hexahedron) in entire domain did not exceed 0.02 m. Distribution of grid elements size on

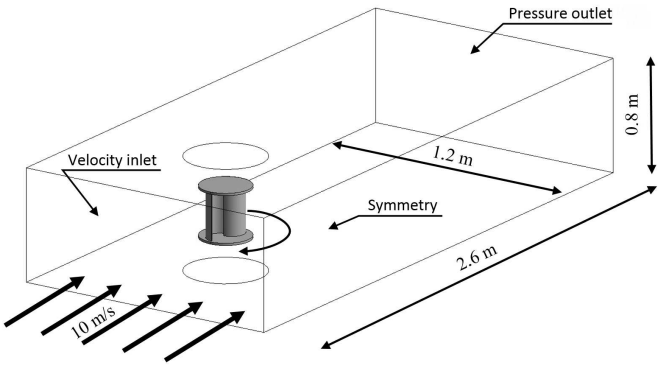

Figure 2: Computational domain.

surfaces were different for different mesh variants and shortly presented in Tab. 1.

The dimensions of the computational domain were determined reducing to the minimum the effect of boundary conditions on the results obtained. Factor, which determines the impact of the size of the flow domain, is the blocking factor (blockage ratio). It is defined as a ratio of the surface area of the object projection normal to the wind direction to the cross-sectional area of the wind tunnel. This factor is commonly used in experimental and computational aerodynamics [6]. Generally, it is accepted that this ratio should not be greater than 7%, which has been preserved in this studies.

Numerical grid was generated using a commercial ANSYS ICEM CFD meshing software. Operation of this mesh generator was automated by means of homemade scripts, allowing easy modifications of parameters of the grid. This facility was used in presented grid dependence studies and will be used in the future to optimize the shape of the turbine rotor.

2.3 Mathematical model

In the applied model, both the pseudosteady state (MRF method) and transient (sliding mesh method) computations used the same computational domain geometry and the same shape of the turbine rotor. All computations and flow postprocessing were performed using the commercial software package for computational fluid dynamics (CFD) ANSYS Fluent [13]. Because of low velocity of fluid passing around turbine (Mach number, $\mathrm{Ma} \ll 1$), the fluid in simulations was treated as incompressible medium. Moreover, due to large computational domain and limited resources, the

equations describing the motion of the fluid were Reynolds ensemble averaged resulting in the so called RANS (Reynolds averaged Navier-Stokes) set of equations for stationary model (MRF) and URANS (unsteady Reynolds averaged Navier-Stokes, see [7]) set of equations for non-stationary (sliding mesh) model. In order to obtain RANS set of equations for steady state flow, in this paper this is represented as a MRF approach applied to wind turbine rotor motion, one assumes, that instantaneous velocity vector and pressure can be decomposed into average value and fluctuation:

$$\mathbf{u}(\mathbf{x},t) = \bar{\mathbf{u}}(\mathbf{x}) + \mathbf{u}'(\mathbf{x},t) \ , \tag{1}$$

$$p(\mathbf{x},t) = \bar{\mathbf{p}}(\mathbf{x}) + \mathbf{p}'(\mathbf{x},t) \ , \tag{2}$$

where $\bar{\mathbf{u}}(\mathbf{x})$ and $\mathbf{u}'(\mathbf{x},t)$ stands for average velocity vector and its fluctuation, $\bar{\mathbf{p}}(\mathbf{x})$ $\mathbf{p}'(\mathbf{x},t)$ and refers to average pressure and its fluctuation. In context of stationary flows averaging operator $\bar{(.)}$ is understood as a temporal average with averaging period tending to infinity, hence for arbitrary instantaneous flow variable, $\varphi(\mathbf{x},t)$ one writes

$$\bar{\varphi}(\mathbf{x}) = \lim_{T\to\infty}\left[\frac{1}{T}\int_0^T \varphi(\mathbf{x},t)dt\right] \ , \tag{3}$$

$$\varphi'(\mathbf{x},t) = \varphi(\mathbf{x},t) - \bar{\varphi}(\mathbf{x}) \ . \tag{4}$$

Abovementioned definitions fail for inherently unsteady flows, like the sliding mesh formulation of flow around operating wind turbine rotor. In such cases ensemble average in terms of N independent realizations of exactly the same unsteady flow process (with exactly the same unambiguity conditions: geometry, initial and boundary conditions and so on) are used. This results in following definitions for arbitrary flow variable $\varphi(\mathbf{x},t)$:

$$\bar{\varphi}(\mathbf{x},t) = \frac{\sum_{i=1}^{N}\varphi_i(\mathbf{x},t)}{N} \ , \tag{5}$$

$$\varphi'(\mathbf{x},t) = \varphi(\mathbf{x},t) - \bar{\varphi}(\mathbf{x},t) \ , \tag{6}$$

where $\varphi_i(\mathbf{x},t)$ is a single realization of flow variable value, treated in this approach as a random variable. It should be noted that so defined average value is time dependent. Moreover, according to ergodic hypothesis for steady state conditions temporal average and ensemble average tend to the

same value. Due to simplicity, the same notation will be used for average value and fluctuations in the temporal and ensemble sense in further text.

Applying decomposition described by equations (1)–(4) to the set of Navier-Stokes equations results in so called RANS formulation. Applying of decomposition described by formulas (1)–(2) and (5)–(6) to set of flow equations results in URANS formulation. Assuming incompressible, isothermal flow and applying Reynolds decomposition using ensemble average operator, one obtain URANS set of equations as follows:

$$\nabla \bar{\mathbf{u}} = 0 \,, \tag{7}$$

$$\rho \left(\frac{\partial \bar{\mathbf{u}}}{\partial t} + \bar{\mathbf{u}} \, \nabla \bar{\mathbf{u}} \right) = -\nabla \bar{p} + \mu \nabla^2 \bar{\mathbf{u}} + \nabla \boldsymbol{\tau}^R \,. \tag{8}$$

In case of RANS formulation set of flow equations is similar except the unsteady term in the momentum equation (8), which disappears in RANS approach due to temporal averaging. Hence, RANS equations is not written explicitly in this paper, it has been widely discussed in [8,9]. Application of Reynolds decomposition to unsteady Navier-Stokes equations leads to additional term called the turbulent stress (Reynolds stress) tensor which reads:

$$\boldsymbol{\tau}^R = -\rho(\overline{\mathbf{u}'\mathbf{u}'}) \,. \tag{9}$$

This tensor is defined as an average dyadic product of velocity fluctuation vectors and can be interpreted as an average covariance of velocity oscillations or additional stress due to turbulent mixing of fluid. The Reynolds stress tensor is symmetric, hence it gives additional six unknowns, except pressure and velocity vector. Therefore a set of closing assumptions (formulas) are necessary to close the Navier-Stokes system of equations known as turbulence models. Over the years, many models have been developed for predicting the effects of turbulence on the behaviour of the fluid. The main division of turbulence models includes two groups. The first one uses Bussinesq hypothesis and the concept of turbulent viscosity. Most common models in this group are:

- zero equation models – e.g., Prandtl mixing length model,
- one equation models – e.g., Spallart-Almaras model,
- two equation models – e.g., k-ε model or k-ω model.

The second group consists of models that assume anisotropic nature of turbulence, in which the turbulent stress tensor components are resolved directly, e.g., Reynolds stress model (RSM).

2.3.1 Methodology of modeling of flow around rotating wind turbine

Modeling of fluid flow passing around the wind turbine rotor can be accomplished in several ways. This paper describes two techniques most commonly applied in turbomachinery modeling. The first one, which is considered as the easiest way is so-called: multiple reference systems (MRF) method. In this method, the flow equations in the vicinity of rotating element are written in the rotating reference frame which results in supplementary terms in flow equations responsible for taking into account the effects of acceleration of the fluid like centrifugal or Coriolis forces. It is worth noting that there is no numerical grid movement in the MRF method. Thus, the MRF method is often referred to as a frozen rotor approach. This can be envisaged as a state in which the flow is observed over the moving element frozen in motion. The second method is the sliding mesh. It allows defining the speed and manner of sliding the cell walls to each other. The movement of objects is modelled by mutual 'sliding' of the subdomains over a common area connecting them (so-called interfaces). This method requires longer calculation time due to the fact that the calculations are carried in transient mode. This study compares the results obtained with both methods. The second method is believed to be more accurate in context of vertical axis wind turbines modelling, however it is more computationally expensive comparing to MRF technique.

2.3.2 Boundary conditions and solver settings

Computational domain with distinguished boundary conditions are shown in Fig. 2. At the inflow boundary first type boundary condition, namely known value of velocity vector magnitude and direction normal to boundary, was prescribed. At the outflowing boundary known value of static pressure and zero derivative of velocity in the direction normal to boundary is assumed. This is boundary condition type commonly used at the outflowing surface. At the side surfaces zero shear stress and pressure derivative in the normal direction to boundary was prescribed. This type of boundary condition very well corresponds to the conditions existing during incompressible air flow around body.

Model equations were spatially discretised with second scheme for all variables except pressure. Pressure field was discretised with staggered grid technique (PRESTO – pressure staggered grid) for unstructured grids [14].

Pressure-velocity coupling of incompressible flow equations were treated with SIMPLE (semi-implicit method for pressure linked equations) algorithm, which works very well for most type of flows on high quality grids [15]. Final set of discretised equations were solved with fully segregated (iterative) pressure based solver. In case of unsteady simulation first order implicit time discretisation was used.

3 Results

Usually operation conditions of wind turbines are described by two dimensionless parameters. The first one named as a tip speed ratio (TSR) and the second one is the Reynolds number, defined for the rotor diameter. TSR parameter describes the ratio of the turbine blades tip movement speed to the undisturbed fluid velocity, and can be written as follows:

$$\lambda = \frac{\omega D}{2w} \,, \tag{10}$$

while the rotor Reynolds number can be written as

$$\mathrm{Re} = \frac{wD}{\nu} \,, \tag{11}$$

where, D stands for the rotor diameter, w stands for the magnitude of undisturbed wind velocity and ω is the rotor rotational speed and finally ν refers to the kinematic viscosity coefficient. All simulations were performed for one operation point of the turbine. Wind speed was 10 m/s while the rototional speed of rotor was 10 rad/s, and they correspond to the following parameters: $\lambda \approx 0.1$ and the Reynolds number $\mathrm{Re} \approx 1.42 \times 10^5$. Chosen operating point is below optimal operating condition for typical vertical axis wind turbines. However, such an operating point is interesting because it may occur when the turbine is heavy loaded at weak or moderate wind conditions. Furthermore, temporal (or angular) recording of torque at the turbine axis at low TSR value is more complicated than at high TSR values, when it resembles trigonometric function. For this reason low TSR operating point is better for validation purposes than high TSR conditions.

3.1 Influence of the numerical grid on wind turbine torque calculation

The accuracy of the numerical model, as a discrete representation of a mathematical model of the phenomenon, strongly depends on the quality and

density of the numerical grid. The increase of the number of grid elements should lead to increase of the calculation accuracy. However, it also increases the amount of resources needed. Therefore, the optimal numerical grid should be a compromise between the accuracy of the results, and the demand for computing resources.

The influence of the grid was investigated by transient simulation of the turbine operation with application of the Sliding Mesh method. In calculations k-ε realizable turbulence model was used with standard way of modeling the boundary layer. Simulations were performed for seven different variants of numerical grid. Numerical meshes marked as nos. 1, 2 and 3 were relatively coarse meshes without prismatic boundary layer. Size of tetrahedron volume cells was growing with increasing distance from rotor surface at different rates. Overall structure for these meshes as well as boundary region around rotor is presented in Fig. 3.

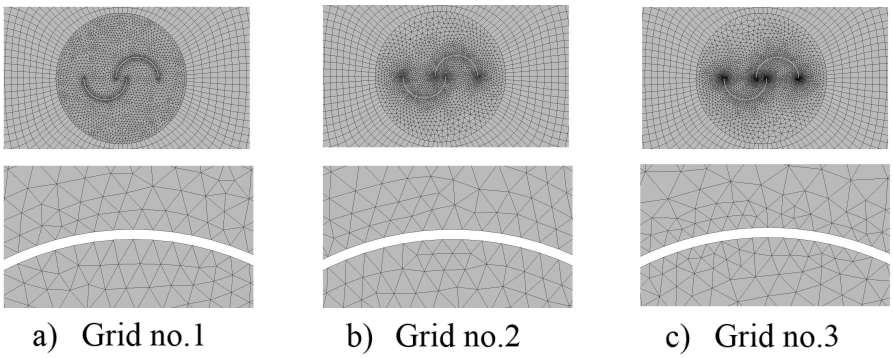

Figure 3: Visualisation of numerical grids with different levels of elements refinement and without boundary layer.

Numerical grids marked by numbers 4 to 7 contained prismatic type boundary layer. Number of prism layers was equal to 3 in case of mesh no. 4. and for further grids (no. 5, 6 and 7) equal to 10. In each case, heights of prisms building particular layers were increasing in geometrical order with multiplication factor equal to 1.2. Total height of boundary layers did not exceed 1.5 height of distance between nodes on surface of the rotor, hence smooth and gradual transition of elements size was assured. Visualization of described above numerical grids is presented in Fig. 4.
Grids with numbers 6 and 7 were structurally nearly identical to grid no. 5 just the total number of elements were increased. For the sake of clarity and convenience, characteristics of all studied grids were collected in Tab. 1.

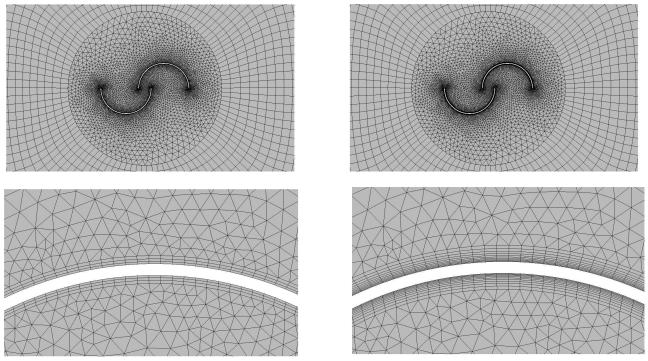

Figure 4: Visualisation of numerical grids with different levels of boundary layer refinement.

Table 1: List of used numerical grids with short characteristic.

Grid number	Number of elements	Range of Y^+ value on wind turbine rotor	Range of node size distribution for surfaces, m	Numerical grid characterization
1	6×10^5	2.28–81.3	0.002–0.2	The base grid with sparse distribution of elements and coarse transition of elements size
2	7×10^5	0.69–75.1	0.002–0.2	Smoothed grid with improved gradation of elements size
3	1.3×10^6	0.61–62.5	0.002–0.2	Smoothed grid with increased density of elements near turbine rotor
4	7.5×10^5	0.13–12.9	0.001–0.2	Smoothed grid with 3 layers of prismatic inflation
5	1.65×10^6	0.05–17.1	0.001–0.2	Smoothed grid with 10 layers of prismatic inflation
6	5.3×10^6	0.05–14.3	0.00075–0.15	Grid no. 5 with globally increased density
7	6.5×10^6	0.04–12.9	0.0005–0.1	Grid no. 5 with globally increased density

Results of calculations of the instantaneous torque induced on the turbine shaft are presented in Fig. 5.

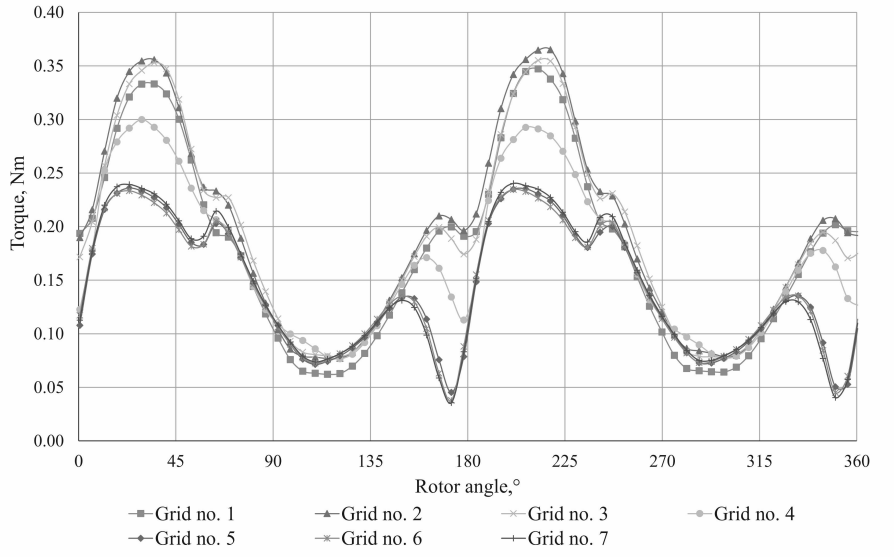

Figure 5: The effect of numerical grid selection on instantaneous torque values for wind turbine.

Analysis of the numerical grid impact revealed that model indicates convergence with gradual increase of grid elements number. Most similar to each other are curves obtained for grids nos. 5, 6 and 7. The differences in mean torque value for these numerical grids do not exceed 2%. Based on calculations performed with use of these grids, it can be concluded that the developed numerical model shows asymptotic convergence of the solution with the grid size. Moreover, it is clearly seen that crucial for obtaining reasonable results is application of adequately refined boundary layer.

3.2 Influence of the time step size

An important parameter of the transient modelling of wind turbines is the time step size. Model sensitivity analysis with respect to the time step size in the simulation of the transient motion of the turbine was carried out for 5 variants. Remaining parameters of the simulations were as follows: numerical grid no. 5 (1.65×10^6 elements) and turbulence model (k-ε realizable). Studies covered 0.01 s, 0.004 s, 0.002 s, 0.001 s, and 0.0005 s

time step sizes, which corresponded to angular displacement of the rotor in each time step respectively: 5.73 °, 2.29 °, 1.15 °, 0.57 °, and 0.29 °. The instantaneous torque values induced on the rotor for different time steps are shown in Fig. 6.

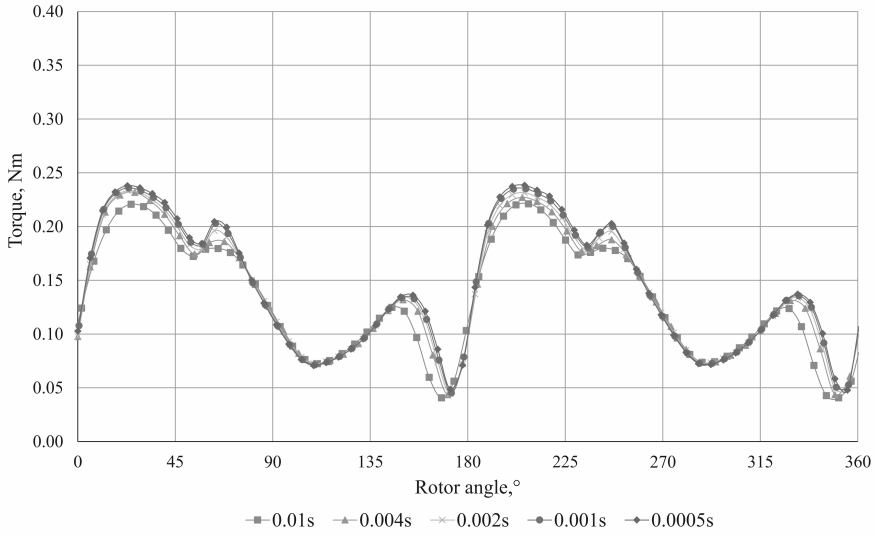

Figure 6: The effect of the time step size on instantaneous torque values for wind turbine.

With the gradual reduction of the time step size asymptotic convergence of the turbine torque is observed. Setting the size of the model time step to 0.001 s seems optimal regarding to required computational effort. Reduction of the time step size twice (to the value of 0.0005 s) causes less than 1% change in the value of calculated instantaneous turbine torque. This, however, results in a double increase in computational effort required. Further calculations were performed assuming the time step size of 0.001 s.

3.3 Influence of the method of rotor movement modeling

Third stage of the study covered the comparison of the torque calculated by two variants of rotor movement modeling namely: MRF and sliding mesh technique. Calculations were performed using the grid chosen in first stage with 1.65×10^6 elements. Comparison of two methods of modelling of rotor movement is presented in Fig. 7. To carry out this comparison, results

with MRF technique were obtained for a number of different rotor positions around the full revolution with the step equal to 0.1 radian (≈ 5.73 °).

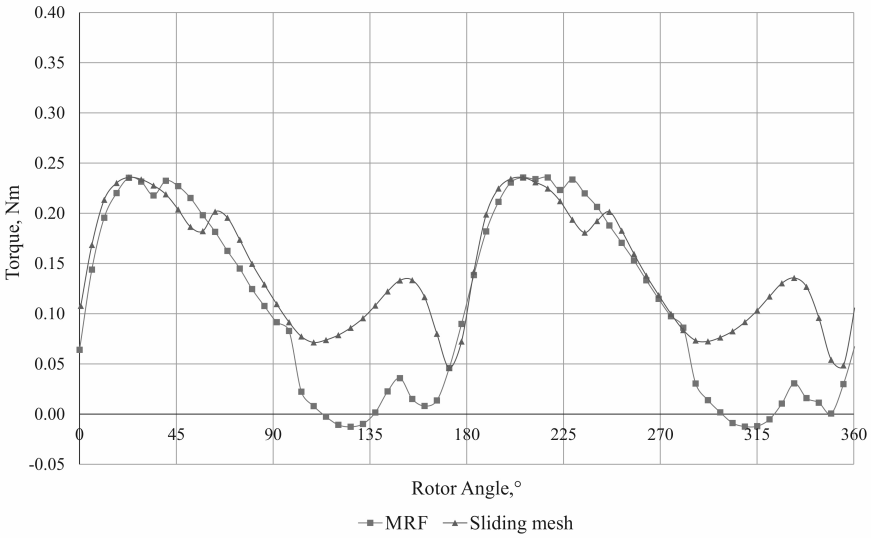

Figure 7: The effect of modeling method selection for description of rotor movement on momentary torque values for wind turbine.

Discrepancies in the calculated torque induced on the turbine shaft indicate that exist significant differences between the flow field representations in both analysed rotor movement models. Particularly, problematic is the moment of reversing direction of accelerated fluid stream inside the turbine rotor. Observable discrepancies between torque curves are highest for rotor deflection range from 110° to 180° and from 290° to 360°. In Fig. 8. comparison of flow fields calculated with both modeling methods of rotor movement for chosen instantaneous rotor angles are shown. For better picture of the problem, chosen rotor angles correspond to the instances at which small as well as significant discrepancies are observed. At the first sight it seems that velocity fields for both modeling techniques are very similar. However, closer examination reveals differences in the flow pattern in the wake behind the turbine rotor. Nevertheless, further examination shows noticeable discrepancies in fluid flow distributions between rotor blades. It can be noticed, that in case of the MRF technique fluid overlapping stream rapidly extinguish with increasing instantaneous rotor angle which appears to not be the case for the sliding mesh technique. Confrontation of the flow

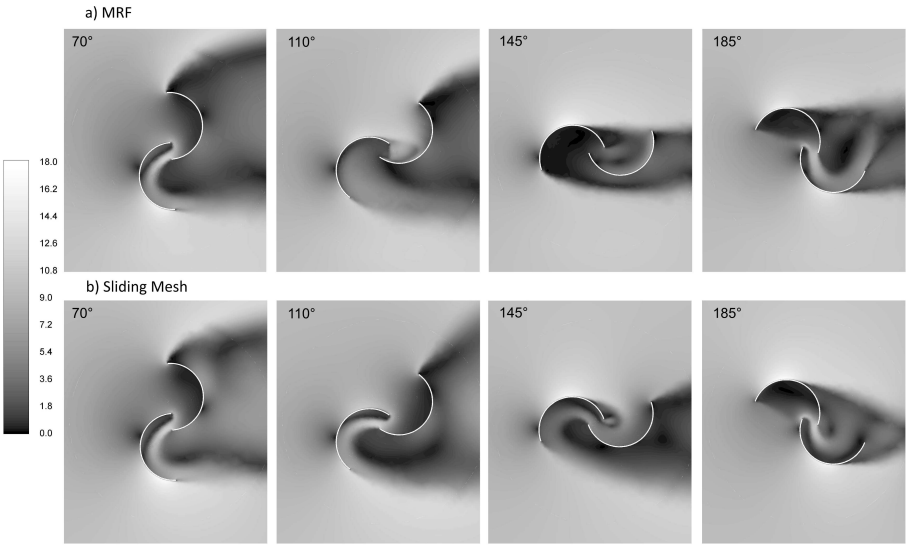

Figure 8: The effect of modeling method selection for description of rotor movement on momentary torque values for wind turbine, velocity magnitude (m/s).

fields with torque plots leads to conclusion that this particular discrepancy is the main source of differences in calculated torque values. In this case fluid stream flowing from one blade to another is highly unstable and alternating in its nature and in fact, it should be considered as an unsteady characteristics of fluid flow. Considering MRF method as a quasi steady state modeling approach such a model response can be sourced in averaged over time character of RANS type of modeling. This suggests that modeling the movement of the turbine with MRF is susceptible to unsteady phenomena that occur locally in the flow field. In contrast, computation with sliding mesh method allows one to calculate more physical shape of flow over propeller. Further studies were carried out for transient state with the sliding mesh method.

3.4 Influence of turbulence model

The fluid flow around vertical axis wind turbine under operation is very complicated, due to coupling of phenomena that occur simultaneously:

- dynamic stall,
- boundary layer separation and vortex shedding,

- flow over airfoil with continuously changing angle of attack,
- flow around wall with dynamically changing curvature (from the point of view of the fluid).

These phenomena directly influence turbine operation and its performance, therefore simulation of this process is challenging. Most important flow phenomena, around turbine rotor, are presented in Fig. 9.

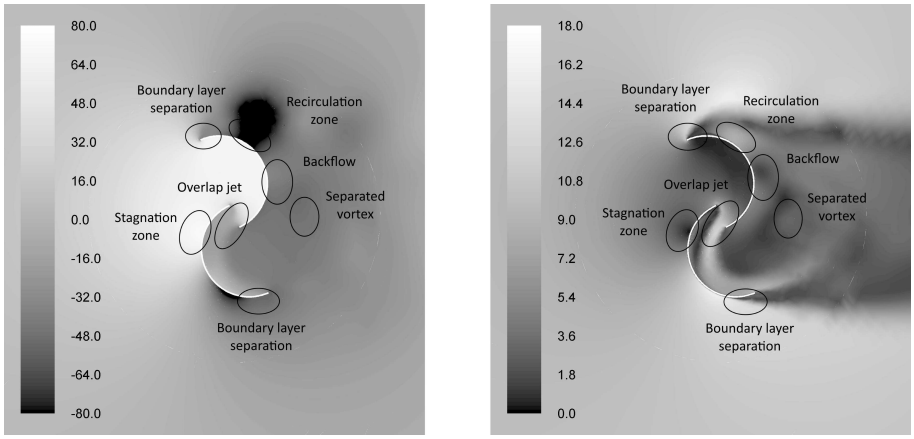

Figure 9: Visualisation of flow phenomena occurring around wind turbine rotor, pressure (Pa) left, velocity (m/s) right.

It is crucial to mention that localisation as well as shape and intensity of displayed flow phenomena differ highly not only depending on turbulence modeling approach. Also rotor deflection has a great impact on their localization, for example stagnation zones or boundary layer separation points. These points dynamically change their size and distribution as rotor deflection progresses.

Even considering that discussed type of wind turbines usually perform with relatively low values of Reynolds number, complex fluid flow is turbulent in its nature. A method of turbulence modelling with usage of the unsteady average fluid flow equations (URANS) comes down to equation set selection for resolving the components of the stress tensor in the fluid. In this study following URANS turbulence models were compared:

- realizable k-ε model with standard wall functions,
- standard k-ε model with enhanced wall treatment,
- k-ω model,

- k-ω SST model,
- SST model.

The calculations were performed for the numerical grid, which showed a very good relation of the accuracy to computation time and guaranteed results of calculations from the area of asymptotic convergence of the model. Detailed description as well as visualization of chosen mesh can be found in Section 3.1. Comparison of turbine torque calculations for different turbulence models is presented in Fig. 10.

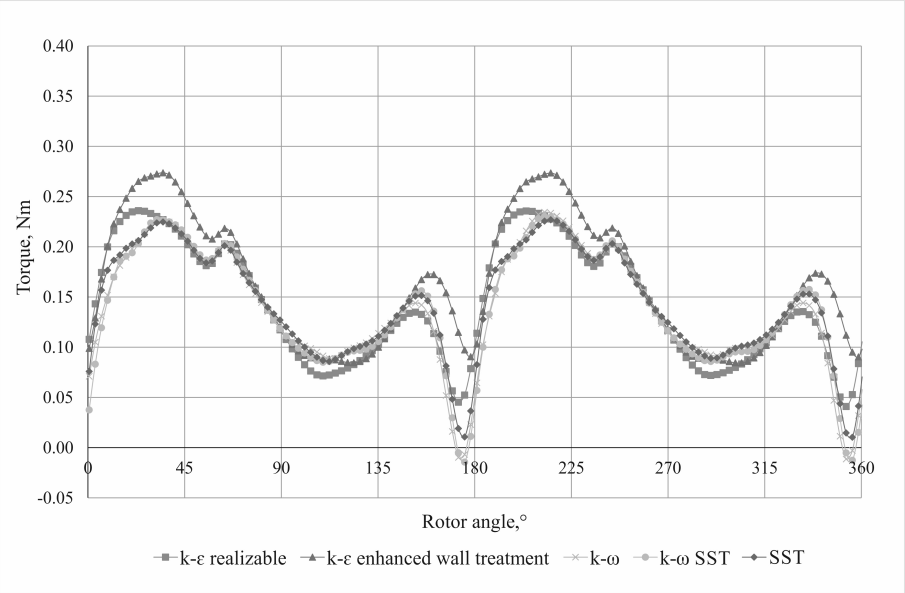

Figure 10: The effect of turbulence model on the computation values of instantaneous torque on the wind turbine shaft.

Despite the wide range of the results some convergence trends can be observed. The application of k-ω, k-ω SST, SST models to describe the flow turbulence result in similar trends of torque curves. Confirmation of these similarities can be found in observation of flow field visualized in Fig. 11. Utilization of all turbulence models to solve fluid flow results in relatively close shape of velocity field, however some significant differences can be noted. Firstly, aerodynamic shade behind the turbine rotor is highly dependent on the turbulence model used. Turbulence models of k-ε type (k-ε realizable and k-ε with enhanced wall treatment) are distinguishing themselves with very different size and shape of lower speed zone behind the

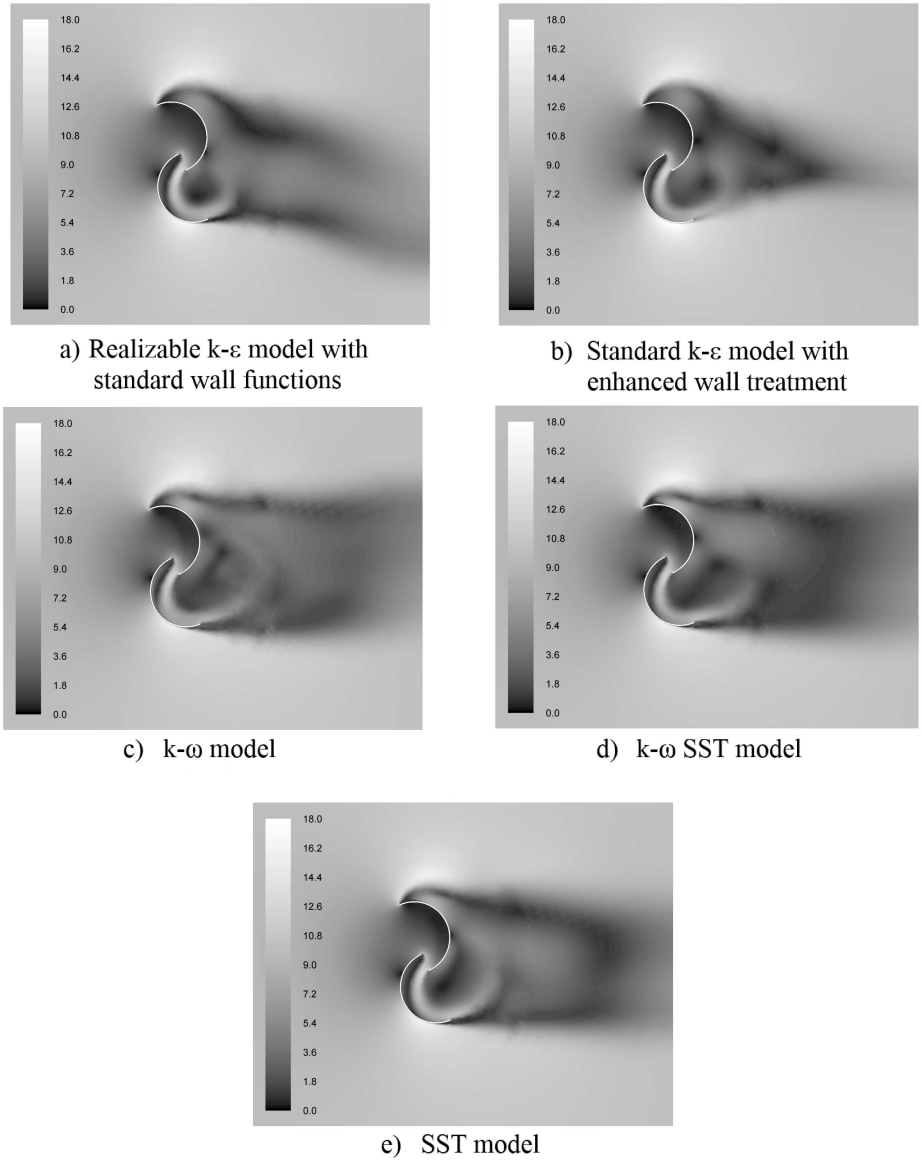

Figure 11: Visualization of velocity magnitude field around wind turbine rotor in its symmetry plane (m/s).

turbine. Secondly, k-ε type models seem to differently calculate behaviour of the boundary layer. If we focus on outside tips of propellers, various

points of boundary layer separation can be noticed. Also models prediction of backflow zones appear to be different.

Comparison of experimental and model values of calculated torque are presented in Tab. 2. Summarizing, the discrepancies between computed, and measured, values of the average torque are very high. This torque prediction discrepancy may have partially its source in the operating point selection. Rapid drop of instantaneous value of torque suggest that wind turbine perform unstable. However, quantification of the comparison between computational and experimental results is impaired because that experimental reference data do not contain information about any friction estimation.

Table 2: List of used numerical grids with short characteristic.

	Experimental	k-ε model with standard wall functions	k-ε model with enhanced wall treatment	k-ω model	k-ω SST model	SST model
Cp	0.025	0.049	0.056	0.039	0.042	0.043
Ct	0.240	0.473	0.540	0.374	0.400	0.416

4 Summary

The most important observations and conclusions:

- Optimal time step size for transient calculation should correspond to the angular displacement of the turbine rotor of about 0.01 rad.
- Properly discretised boundary layer near the rotor surface is crucial for obtaining accurate results of computations.
- Modelling using RANS method does not allow for precise determination of the dynamic phenomena occurring during turbine operation. This is especially manifested at the moments of passing of the stagnation zone over the rotor edge.
- The URANS modelling technique with used turbulence models has indicated tendency to highly overestimate turbine torque at low TSR values.

Received 10 December 2014

References

[1] Burton T., Sharpe D., Jenkins N., Bossanyi E.: *Wind energy handbook*. John Wiley & Sons Ltd, Chicester 2001.

[2] Hau E.: *Wind turbines. Fundamentals, technologies, application, economics, second edition*. Springer-Verlag, Berlin Heidelberg 2006.

[3] Ericsson S., Bernhoff H., Leijon M.: *Evaluation of different turbine concepts for wind power*. Renew. Sust. Energ. Rev. **12**(2008), 1419–1434.

[4] Islam M.R., Mekhilef S., Saidur R.: *Progress and recent trends of wind energy technology*. Renew. Sust. Energ. Rev. **21**(2013), 456–468.

[5] Pope K., Dincer I., Naterer G.F.: *Energy and exergy efficiency comparison of horizontal and vertical axis wind turbines*. Renew. Sust. Energ. Rev. **35**(2010), 2102–2113.

[6] Kamoji M.A., Kedarel S.B., Prabhu S.V.: *Experimental investigations on single stage, two stage and three stage conventional Savonius rotor*. Int. J. Energ. Res. **35**(2008), 32:877–895.

[7] Sagaut P.: *Large Eddy Simulation for Incompressible Flows – An Introduction*. Springer-Verlag, Berlin Heidelberg 1998.

[8] Pope S.B.: *Turbulent Flows*. Cambridge University Press, 2011.

[9] Bradshaw P.: *Turbulence*. Springer-Verlag, Berlin Heidelberg 1976.

[10] Savonius S.J.: *The S-rotor and its applications*. Mechanical Engineering **53**(1931), 333–337.

[11] *Catia VR5R20 Documentation Dassault Systems* 1999–2009.

[12] *ANSYS ICEM CFD 15.0 Userñs manual Southpointe*. Canonsburg (USA) Ansys Inc., 2013.

[13] *ANSYS Fluent 15.0 Userñs manual Southpointe*. Canonsburg (USA) Ansys Inc., 2013.

[14] Patankar S.V.: *Numerical Heat Transfer and Fluid Flow*. Hemisphere, Washington, DC. 1980.

[15] Issa R.I.: *Solution of implicitly discretized fluid flow equations by operator splitting*. J. Comput. Phys. **62**(1986), 40–65.